JOURNAL OF PROPULSION AND POWER
Vol. 23, No. 3, May–June 2007

# Thermal Model of the Hollow Cathode Using Numerically Simulated Plasma Fluxes

Ira Katz,* Ioannis G. Mikellides,† James E. Polk,‡ Dan M. Goebel,§ and Sarah E. Hornbeck¶
*Jet Propulsion Laboratory, California Institute of Technology, Pasadena, California 91109*

DOI: 10.2514/1.21103

**The first results from a hollow cathode thermal model are presented. The thermal model uses the spatially distributed plasma fluxes, calculated by a two-dimensional axisymmetric model of the plasma inside the emitter region, as the heat source to predict the hollow cathode and insert temperatures. The computed insert temperature profiles are compared with measured values for a cathode similar to the 0.635-cm diameter discharge cathode used in the NASA solar electric propulsion technology applications readiness ion engine. The insert temperatures can be used to predict cathode life from barium depletion. The present results and related experimental studies yield three important conclusions. First, the emitter in the NASA solar electric propulsion technology applications readiness hollow cathode does not operate in the emission-limited regime. The thermionic electron current is about 20 A higher than the discharge current and requires significant reverse electron flux from the plasma to satisfy current continuity. Second, the high-plasma density near the centerline of the cathode results in power deposition on the orifice plate that is more than twice the emitter power deposition. Third, despite a higher heat load to the orifice plate, the operating temperature where it would be measured by a thermocouple is approximately 100°C lower than the emitter. The lower orifice plate temperature is due to poor thermal contact between the emitter and the cathode tube and higher than anticipated radiative losses from the external surface of the heater.**

## Nomenclature

| | | |
|---|---|---|
| $F$ | = | geometrical configuration factor |
| $IP$ | = | ionization potential, V |
| $j_{\text{emission}}$ | = | emission current density, $\text{A}/\text{m}^2$ |
| $j_e^{\text{the}}$ | = | plasma thermal current density, $\text{A}/\text{m}^2$ |
| $j_i$ | = | plasma ion current density, $\text{A}/\text{m}^2$ |
| $\dot{q}_{\text{rad}}$ | = | heat loss by radiation, $\text{W}/\text{m}^2$ |
| $\dot{q}_{\text{emission}}$ | = | heat loss by electron emission, $\text{W}/\text{m}^2$ |
| $\dot{q}_e$ | = | heating by plasma electrons, $\text{W}/\text{m}^2$ |
| $\dot{q}_i$ | = | heating by plasma ion flux, $\text{W}/\text{m}^2$ |
| $T$ | = | material temperature, K |
| $T_e$ | = | plasma electron temperature, eV |
| $WF$ | = | emitter work function, eV |
| $\delta_{ij}$ | = | Kronecker delta |
| $\varepsilon$ | = | material emissivity |
| $\kappa$ | = | material thermal conductivity, $\text{W}/\text{m} \cdot \text{K}$ |
| $\sigma$ | = | Stephan–Boltzman constant, $\text{W}/\text{m}^2 \cdot \text{K}^4$ |
| $\phi_{\text{sheath}}$ | = | sheath potential, V |

## Introduction

HIGH-POWER, long-life electric thrusters were considered necessary as NASA planned many of the challenging missions under the Prometheus program. These missions might have required an increase in both life and emission current compared with hollow cathodes used on NASA's Deep Space 1 spacecraft. Although both the discharge and neutralizer hollow cathodes were operating at the end of the NASA solar electric propulsion technology applications readiness (NSTAR) thruster 30,000-h extended life test [1], the future missions may be even more challenging. A previous life test of the International Space Station plasma contactor hollow cathode [2] ended after 28,000 h, when the cathode would no longer ignite. One scenario for end of life is when the insert can no longer provide free barium to lower the work function and the remaining barium in the cathode is tied up in tungstates. It has already been shown that impregnated insert barium depletion rates in xenon-fed hollow cathodes are closely correlated to barium depletion rates in the conventional impregnated cathodes used by the traveling tube industry [3], allowing for the use of a large database of measurements from that community. This previous work assumed that the cathode temperatures were known by measurements. Several previous researchers have investigated hollow cathode thermal processes both experimentally and analytically [4–8]. The hollow cathode thermal model of Van Noord [9] is very similar in approach to the present work, however, it relies on plasma parameters measured along the centerline as measured by Sahli [7]. In this article, we present the first results from a hollow cathode thermal model that uses the spatially distributed plasma fluxes and sheath potentials along the cathode walls as calculated by the two-dimensional axisymmetric model of the plasma (and neutral gas) inside the insert region, developed by Mikellides et al. [10,11]. Unlike the plasma fluxes used by Van Noord [9], the calculations by Mikellides et al. [10,11] show substantial heating due to energetic electrons returning to cathode surfaces. These fluxes are used as the heat source for the thermal model, which is in turn used to predict the hollow cathode and insert temperatures. The computed insert temperature profiles are compared with measured values for a cathode similar to the NSTAR discharge cathode. Once fully validated, the insert temperatures may be used in the aforementioned barium depletion models to predict the insert life before cathode fabrication and test, and to predict the variation of life over a range of operating conditions.

The two-dimensional hollow cathode plasma model [10,11] self-consistently solves the ion, electron, and neutral mass continuity, momentum, and energy equations. The interactions with the hollow

Received 13 November 2005; revision received 5 June 2006; accepted for publication 18 September 2006. 

*Group Supervisor, Advanced Propulsion Technology Group, 4800 Oak Grove Drive, Pasadena, CA 91109, Mail Stop 125-109. Senior Member AIAA.

†Member Technical Staff, Advanced Propulsion Technology Group, 4800 Oak Grove Drive, Pasadena, CA 91109, Mail Stop 125-109. Member AIAA.

‡Section Staff, Thermal and Propulsion Engineering Section, 4800 Oak Grove Drive, Pasadena, CA 91109, Mail Stop 125-109. Member AIAA.

§Section Staff, Thermal and Propulsion Engineering Section, 4800 Oak Grove Drive, Pasadena, CA 91109, Mail Stop 125-109. Senior Member AIAA.

¶Summer Student.

cathode insert region surfaces are through a sheath that attracts electrons from the emitter, and accelerates plasma ions to the walls. The sheath also acts as a barrier that prevents most plasma electrons from returning to the emitter. Electrons are emitted using the Richardson–Dushman equation for thermionic emission [12], which includes Schottky enhancement due to sheath fields. If a measurement exists, the emitter temperature in the plasma model is specified (and held fixed) during the plasma calculation, otherwise it is determined by iteration. For the calculation of the plasma inside the emitter region of the NSTAR cathode, the measured emitter temperature profile was used. Emitted electrons cool the cathode by the work function. Incident ions heat the wall by their kinetic energy (sheath and presheath potentials) plus the ionization energy minus the work function. The work function is a cooling effect because ions that reach the emitter are neutralized by removing electrons from the emitter. Returning electrons heat the walls by their kinetic energy and the work function. These plasma fluxes are used as source terms in the thermal model.

The two-dimensional thermal model has been designed to allow for the accurate representation of the interface fluxes between the various cathode components. Thermal transfer processes include bulk conduction, interface conduction, and radiation. The code is imbedded in an Excel spreadsheet, and the cathode geometry is entered graphically. Steady-state temperatures are calculated in under a minute. Radiation from the orifice plate and other parts of the cathode is the primary heat loss mechanism. Results from the calculations are compared with insert temperature measurements taken in a hollow cathode during operation with xenon flow.

## Background

A hollow cathode is a device that provides amperes of electrons to ionize neutrals (discharge cathode) or neutralize the thrust-producing ion beam (neutralizer cathode). Both types of cathodes share the same design, consisting of a hollow tube capped at the end with a plate with a small orifice. The tube wall immediately upstream of the orifice plate is lined with barium-impregnated sintered tungsten that serves as a low work function thermionic electron emitter. Xenon gas flows through the cathode and is partially ionized by electrons from the emitter. The ions both neutralize the space-charge of the emitted electrons and serve to heat the emitter. Electrons, ions, and neutral particles leave the orifice and enter the neighboring discharge chamber or ion beam expansion region.

The two-dimensional, time-independent plasma code was developed to identify those mechanisms that affect the life of the emitter [10,11]. The objective was to develop a theoretical model that predicts the steady-state, two-dimensional distributions of all pertinent plasma properties, including electron and ion fluxes, and the sheath potential along the emitter. The geometrical simplicity of the emitter region (see Fig. 1a) allows us to focus on accurately developing and validating the complex physics associated with the neutral and ionized gases in the presence of electron emission from the insert surface. Also, the absence of time-dependent terms in the plasma conservation equations and the neglect of neutral gas dynamics simplify the numerical approach and reduce the computational times required to attain the steady-state solution.

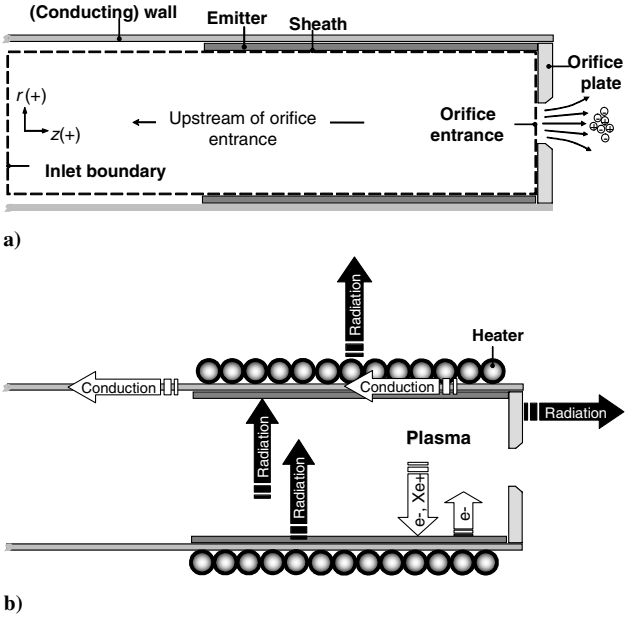


**Fig. 1 Hollow cathode schematic: a) region simulated by two-dimensional plasma model is defined by dashed line, and b) thermal model sources and sinks.**

## Thermal Model

The hollow cathode thermal model is a two-dimensional computer code that uses the ion and electron fluxes from the plasma model mentioned previously as input to predict the temperature distribution in the cathode. A sample problem geometry modeled by the thermal code is shown in Fig. 2. The orifice plate is located at the right of the model. The bottom of the figure represents the centerline of the axisymmetric geometry. Positive numbers identify different materials (e.g., the number one identifies the emitter material) and negative numbers are used to identify radiative boundary conditions (e.g., $-2$ is associated with radiative transport properties of the cathode tube). The code models heat conduction and radiation in a simple geometrical representation of a hollow cathode. The purpose of the code is to provide a fast (calculations take less than a minute) assessment of how insert plasma thermal fluxes influence the cathode insert and orifice plate temperatures. The code includes thermal conduction, radiative heat losses, and, within the insert region, radiative heat transfer. It does not include plasma radiation, which is assumed small, because the resonant xenon lines are optically thick in the line centers [13]. A schematic of the thermal fluxes modeled is shown in Fig. 1b.

The heat conduction equation within the hollow cathode materials is solved using radiation and plasma heat flux sinks and sources.

$$\oint \kappa \nabla T \cdot \mathrm{d}\boldsymbol{S} = \oint \dot{q}\, \mathrm{d}S \tag{1}$$

The temperatures are computed for cathodes in self-heating operation using the plasma fluxes and emission currents calculated by the plasma code. The heat sources are

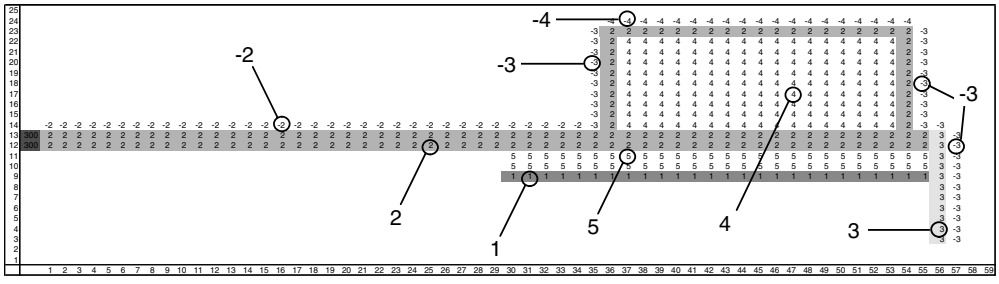


**Fig. 2 Input geometry for the hollow cathode thermal model.**

$$\dot{q} = \dot{q}_{\text{rad}} + \dot{q}_{\text{emission}} + \dot{q}_e + \dot{q}_i \tag{2}$$

where

$$\dot{q}_{\text{rad}} = -\varepsilon\sigma T^4 \tag{3}$$

$$\dot{q}_{\text{emission}} = -j_{\text{emission}} WF \tag{4}$$

$$\dot{q}_e = -j_e^{\text{th}} e^{-\phi_{\text{sheath}}/T_e}(2T_e + WF) \tag{5}$$

$$\dot{q}_i = -j_i\left(\phi_{\text{sheath}} + \frac{1}{2}T_e + IP - WF\right) \tag{6}$$

Emitted electrons cool the insert by the work function, approximately 2 eV per electron, which is calculated as a function of temperature [14]. The work function and the sheath potentials are calculated self-consistently in the plasma code, because the emitted electron current density is very sensitive to the work function and the sheath must adjust to provide the measured cathode current. In the thermal model, which uses as input calculated plasma currents, the work function enters only linearly and because the work function varies only a few percent over the insert, a constant value was used. Backflowing plasma electrons heat the emitter by the work function and the flux weighted average electron kinetic energy, which for an isotropic half Maxwellian is twice the electron temperature as shown by Eq. (7).

$$\begin{aligned} f(v_x, v_y, v_z) &= n\left(\frac{m}{2\pi eT}\right)^{\frac{3}{2}} e^{-\frac{m}{2eT_e}\left(v_x^2+v_y^2+v_z^2\right)}\,\mathrm{d}^3\boldsymbol{v} \\ \langle KE\rangle &= \frac{\iiint f(\boldsymbol{v})\left(\frac{1}{2}m\boldsymbol{v}\cdot\boldsymbol{v}\right)\mathsf{v}_z\,\mathrm{d}^3\boldsymbol{v}}{\iiint f(\boldsymbol{v})\mathsf{v}_z\,\mathrm{d}^3\boldsymbol{v}} \\ &= \frac{eT_e\iiint e^{-s^2}s^2 s\cos\theta s^2\,\mathrm{d}s\,\mathrm{d}\cos\theta\,\mathrm{d}\phi}{\iiint e^{-s^2}s\cos\theta s^2\,\mathrm{d}s\,\mathrm{d}\cos\theta\,\mathrm{d}\phi} = \frac{eT_e\int_0^\infty e^{-s^2}s^4\,\mathrm{d}s^2}{\int_0^\infty e^{-s^2}s^2\,\mathrm{d}s^2} \\ &= 2eT_e \end{aligned} \tag{7}$$

The ion kinetic energy includes acceleration across the local sheath as well as the ion thermal energy. The thermal fluxes are input in tabular form along the axial length of the emitter and radius along the upstream surface of the orifice plate. The heat flux inside the orifice channel is presently assumed to be of the same magnitude as the heat flux to the upstream orifice plate surface at the entrance to the orifice.

The code is written in Visual Basic for Applications and is run within an Excel spreadsheet. The code employs a regular R–Z mesh with fixed cell sizes $\Delta R$ and $\Delta Z$. The hollow cathode geometry is defined graphically by entering the material number, a positive integer, into the spreadsheet. The code interprets one as the emitter material, two as the tube, and three as the orifice plate. The material number is associated with a value for the thermal conductivity. The upstream boundary temperature is entered into the leftmost column. Exterior surfaces that lose heat by radiation are indicated by a negative integer in the neighboring cell. A 0 K background is assumed. Emissivities of the insert and the upstream side of the orifice plate are tied to their material numbers. The cathode heater is treated as metal cylinder filled with a weakly conducting material. Emission from the ends of the heater, its metal foil wrap, and conductive losses through the heater sheath and leads are all lumped together in the code as radiative losses with an effective emissivity of 0.2. This value is much higher than polished tantalum foil, but lower than the heater sheath material, and also accounts for conductive losses through the leads. Presently, the model does not include provisions for a keeper.

The steady-state thermal transport equation is solved by the method of successive overrelaxation (SOR). About 1000 iterations are required to reach a solution, taking less than a minute on a notebook personal computer. Radiative heat transfer in the insert region is modeled as radiation in an enclosure of diffuse-gray surfaces [15]

$$\sum_{j=1}^{N}\left(\frac{\delta_{kj}}{\varepsilon_j} - F_{k-j}\frac{1-\varepsilon_j}{\varepsilon_j}\right) = \sum_{j=1}^{N} F_{k-j}\sigma\left(T_k^4 - T_j^4\right) \tag{8}$$

where $F_{k-j}$ is the configuration factor between two annular ring surfaces of the emitter, or an annular ring emitter surface and the orifice plate. The radiative heat transfer is calculated by inverting these enclosure equations during each SOR iteration.

## Results

A sample calculation with the thermal model that used the plasma fluxes calculated by the plasma model for the NSTAR operating condition of 12 A and 0.42 mg/s [11] is presented in this section. The plasma density profile along the axis of symmetry is compared with a laboratory measurement [16] in Fig. 3. Emission enhancement and emission turnoff are both included in the plasma model result. The error associated with the plasma density measurement is ±40–50%. Calculated plasma density and plasma potential contour maps are shown in Fig. 4. It is noted that the plasma density drops by an order of magnitude within 2 mm of the orifice plate, and that the density and potentials near the wall differ substantially from the centerline values.

The 12 A net cathode current resulted from almost 32 A of electron emission by the insert countered by 20 A of plasma (thermal) electrons back to the insert and the orifice plate. The backflowing electron current is modeled as the one-sided plasma electron thermal flux reduced by the local sheath potential through the Boltzmann factor in Eq. (5). Only about 0.5 A of the net cathode current is due to electrons that are generated by the ionization of the xenon gas (see Table 1).

The calculated thermal fluxes to the insert are shown in Fig. 5. The net thermal power to the insert is about 13 W and is the result of near cancellation of cooling by electron emission and heating from absorption of plasma thermal electrons. Ions contribute about 4 W to the insert heating. Radiation from the plasma is ignored, because the xenon resonance lines are optically thick in the line centers, and most of energy is returned to the electron fluid. The sheath potential prevents plasma electron thermal conduction with the cathode walls. The bulk of the heating is along the orifice plate, where, due to the high work function, the emission cooling is small. The components of the thermal flux to the orifice plate are shown in Fig. 6. It is noted that near the orifice, ion heating becomes significant, which is due to both the high plasma density and the high sheath potential in this region. The thermal flux density to the inside wall of the orifice is assumed to be the same as the flux density to the orifice plate

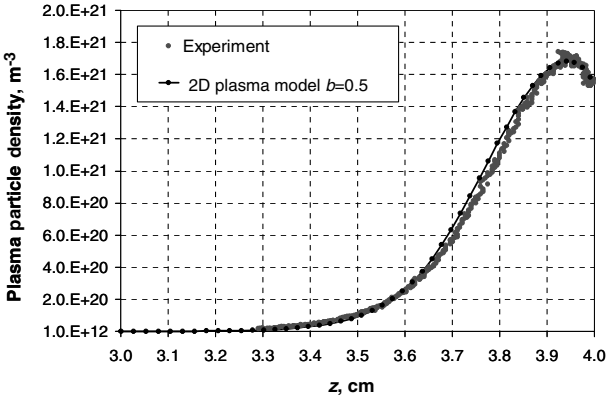


**Fig. 3 Comparison between measurement and theory for plasma particle density along axis of symmetry of NSTAR cathode.**

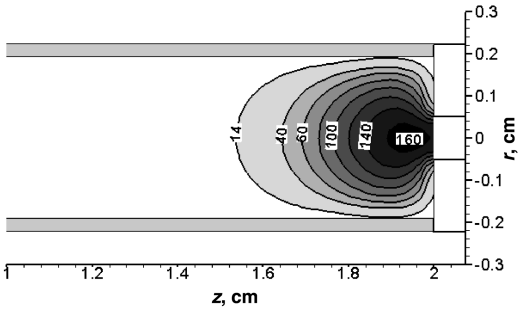


a) Plasma particle density (units of 1.0e10m$^{-3}$)

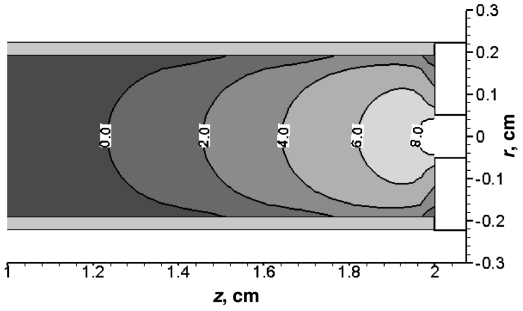


b) Plasma potential in volts (computed by 2-D plasma model)

**Fig. 4 Calculated plasma density and plasma potential contour maps.**

upstream surface at the orifice radius. The combined orifice plate upstream surface and orifice interior heating is more than twice that of the insert alone. The integrated flux values that represent the emitter and orifice plate heating are shown in Table 2. They were obtained after interpolating the two-dimensional plasma model values onto the hollow cathode thermal model geometry (Fig. 1).

It is found that the thermal model results are sensitive to the orifice plate emissivity. The value for tungsten emissivity has been taken as 0.21. This value is higher than the reported value for polished tungsten [17], 0.175, and has been adjusted to best fit the measurements. Although slightly higher than the polished tungsten value, it is lower than measured values for rough, porous tungsten [18]. The thermal model does not include the variation of emissivity with temperature. The orifice plate of the cathode used in the experiments was textured by ion bombardment (a natural evolution from the original machined surface that is observed in all cathodes after several hundred hours of operation), and had a surface roughness intermediate between polished and porous tungsten. The value of emissivity chosen to reproduce the measured orifice plate temperature is therefore not unreasonable. The peak orifice plate temperature in the calculation is 1420 K, and occurs at the center of the orifice plate. A comparison between values measured by thermocouples on the cathode (see Fig. 7) and calculated values are shown in Table 3. The case is for a discharge current of 12 A. (Note that the code uses the measured TC4 temperatures shown in Table 3 as a boundary condition, and thus the exact agreement.) The orifice plate thermocouple is attached at the outer radius of the orifice plate, which is cooler than the center. The most significant result of the calculation is that the overall trend in temperature is in rough agreement with the measurements. Internal and external temperatures were measured on a cathode with the same geometry as the NSTAR cathode operated at the same conditions modeled with the plasma model. External temperatures measured with W–*Re* thermocouples on the cathode tube near the orifice plate and just upstream of the heater coil are listed in Table 3.

**Table 1 Components of the net hollow cathode current**

| Source | Current, A |
|---|---|
| Emitted electrons | 31.7 |
| Absorbed electrons | 20.2 |
| Absorbed ions | 0.5 |
| Net | 12 |

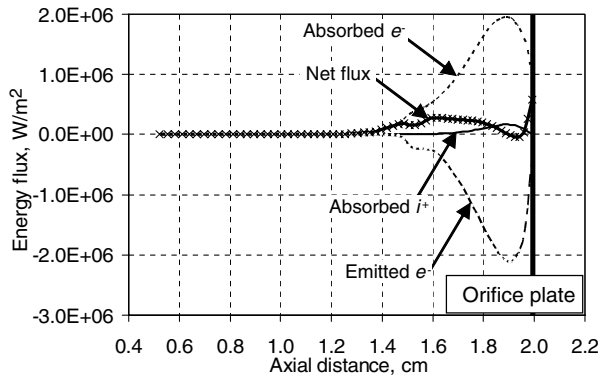


**Fig. 5 Components of plasma energy flux to insert emitter surface.**

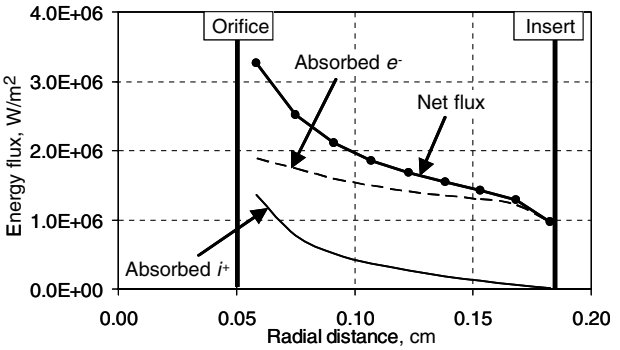


**Fig. 6 Components of plasma thermal flux to upstream surface of orifice plate.**

The axial temperature distribution on the emitting surface inside the cathode is displayed in Fig. 8. The temperature was measured using a fast scanning fiber optic probe and a two-color pyrometer system. An optical system employing narrow bandpass interference filters was used to eliminate plasma line radiation and measurement at two discrete wavelengths allowed the use of ratio pyrometry to minimize source-detector geometry effects. The system was calibrated in situ using the hollow cathode heater and thermocouples on the orifice plate, which compensates for cavity and surface effects on the effective emittance. Extensive testing demonstrated that the measurements were repeatable at a given operating point to within 1–2°C. In regards to the thermocouples, under nearly isothermal conditions during calibration, the readings agreed to within 2°C. During cathode operation, however, they differed by 10–15°C. A more detailed description of the system and methods used for the measurements is provided in [19,20]. Results from an earlier test with a different insert and slightly lower flow rate are also plotted and show similar behavior. The temperature peaks at about 1200°C at the downstream end of the insert and drops by 200°C along the emitter.

The calculated temperature along the insert surface is also shown in Fig. 8. It is noted that the temperature profile flattens within a few millimeters of the orifice plate where most of the heat input occurs. A measurement by a thermocouple that was placed on the side of the orifice plate facing the anode, at a radius near that of the emitter, indicates that the peak insert temperature is about 100°C higher than the temperature of the orifice plate, even though the orifice plate power input is 2.4 times higher than that into the emitter. This is an indication of poor thermal contact between the emitter and the tube

**Table 2 Insert surface and orifice plate heating**

| Heating of | Power, W |
|---|---|
| Insert surface | 12 |
| Orifice plate | 29 |

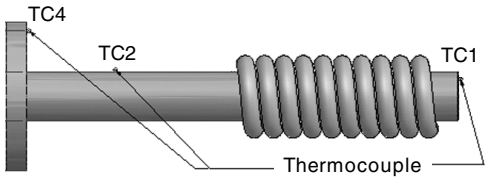


**Fig. 7 Location of thermocouples on the test cathode.**

that surrounds it, necessitating large temperature differences to reject the input heat flux. Poor contact is expected in this geometry because the emitter outer diameter is slightly smaller than the inner diameter of the cathode tube, resulting in a gap of about 100 $\mu$m between the two surfaces. Even in regions where the insert is resting on the tube wall, the rough surface of the porous tungsten results in a small contact area. Initially, the primary heat conduction mechanism between these two components is radiation. After long periods of operation, the gap between the tube and the emitter fills with barium oxide released from the impregnant [1,21], which has a very poor thermal conductivity. In the thermal model, this coupling is modeled using an effective interface conductivity. Radiative coupling at the expected temperatures yields an interface conductivity of approximately 150 $W/m^2 \cdot K$, and conduction through barium oxide increases this conductivity to about 400 $W/m^2 \cdot K$. Agreement between the measured and calculated peak insert temperatures shown in Fig. 8 was achieved with an interface conductivity of 300 $W/m^2 \cdot K$, which is consistent with the radiative coupling and some conduction through contact points or barium oxide deposits. The reason for the differences between the shape of the measured and calculated temperatures near the emitter tip are not understood.

In addition to the preceding assessment of the relative heating of the cathode insert and orifice plate, it is also constructive to examine where the heat is lost. Although the orifice plate is the hottest surface, it has a small area. The calculation shows that only about 5 W are radiated away from the orifice plate. About half of the power is removed by the heater coils due to their large radiating area at the ends of the coils and good conduction path through the leads. About 10 W are conducted through the tube to the upstream mount.

## Discussion

The thermal model calculations show the sensitivity of hollow cathodes on the emissivity of the orifice plate and on the thermal contact between the emitter and the tube. Table 4 compares the model results with the adjusted orifice plate emissivity and with the literature value for polished tungsten. The fractional change in the peak absolute temperature is about one fourth of the change in emissivity. This is consistent with the conclusion that most of the cathode heat is lost by radiation, because the radiative power varies only linearly with the emissivity, but to the fourth power in temperature. However, a difference of 50°C, although only about a 5% change in emitter temperature, has major consequences on insert impregnate life and electron emission.

**Table 3 Comparison of measured thermocouple temperatures with model results using adjusted tungsten emissivity of 0.21**

| Thermocouple | Measured, °C | Thermal model, °C |
|---|---|---|
| TC1 | 1092 | 1096 |
| TC2 | 715 | 720 |
| TC4 | 284 | 284 |

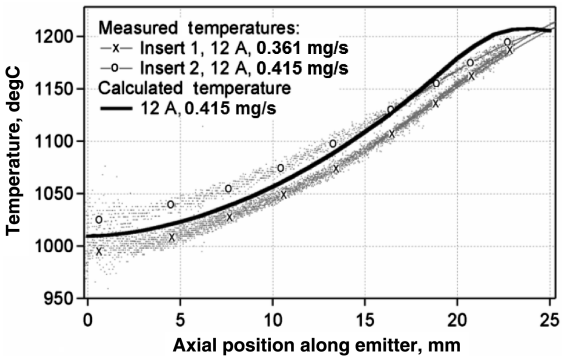


**Fig. 8 Measured emitter temperatures compared with calculated values. Thermal model simulation performed for insert 2.**

**Table 4 Comparison between thermocouple temperatures calculated using adjusted and polished tungsten values for orifice plate emissivity**

| | Adjusted, °C | Polished, °C |
|---|---|---|
| Emissivity | 0.21 | 0.175 |
| TC1 | 1096 | 1146 |
| TC2 | 720 | 758 |
| TC4 | 284 | 284 |

With the preceding sensitivities in mind, the thermal model presented in this article reproduces the axial variations of both the insert and the tube temperatures. The results from the combined plasma thermal model provide insight into the operation of the NSTAR discharge hollow cathode. The insert region plasma calculation, which has been validated with experiment measurements, shows that the insert was not operating in an emission-limited regime. The emitted current was almost three times the circuit current. Most of the emitted current was balanced by the plasma electron current returning to the cathode surfaces. The sheath potential adjusts to control the return electron current to maintain the circuit current. The exponential dependence of the return current on the sheath potential gives the hollow cathode its nearly vertical current-voltage characteristic. This result has important implications on hollow cathode life because all cathode insert failure modes are strongly dependent on the operating temperature. Conceivably, with an improved thermal design, the required discharge current could be emitted at lower operating temperatures, yielding improved life, but probably at the expense of a slightly higher cathode sheath voltage.

In the NSTAR-like cathodes, the relatively small orifice leads to high electron current density and internal pressure, which results in a very short emission zone and high plasma densities at the downstream end, particularly near the centerline. The combination of these high densities and a sheath voltage sufficiently low to allow significant reverse electron flow yields very high orifice plate heat loads. The thermal analyses suggest that these heat loads are rejected largely by radiation from the heater assembly. This also has interesting implications for cathode thermal design trades. Improved radiation shielding to decrease losses during heater operation will result in higher cathode temperatures during operation with a discharge.

Finally, poor thermal contact between the emitter and the cathode tube results in large temperature differences between these components. Improved thermal contact at this interface would result in lower emitter temperatures for a given circuit current.

## Acknowledgments

The research described in this paper was carried out by the Jet Propulsion Laboratory, California Institute of Technology, under a contract with the National Aeronautics and Space Administration for the Prometheus Advanced Systems and Technology Office. Portions have been presented as Paper 2005-228 at the International Electric Propulsion Conference, Princeton, New Jersey, November 2005.

## References

[1] Sengupta, A., Brophy, J. R., and Goodfellow, K. D., "Status of the Extended Life Test of the Deep Space 1 Flight Spare Ion Engine After 30,000 Hours of Operation," AIAA Paper 03-4558, July 2003.

[2] Sarver-Verhey, T. R., "Destructive Evaluation of a Xenon Hollow Cathode After a 28,000 Hour Life Test," AIAA Paper 98-3482, July 1998.

[3] Goebel, D., Katz, I., Polk, J. E., Mikellides, I. G., "Extending Hollow Cathode Life for Electric Propulsion in Long-Term Missions," AIAA Paper 04-5911, Sept. 2004.
[4] Mirtich, M. J., and Kerslake, W. R., "Long Lifetime Hollow Cathodes for 30-cm Mercury Ion Thrusters," AIAA Paper 76-985, Nov. 1976.
[5] Domonkos, M. T., Gallimore, A. D., and Patterson, M. J., "Thermographic Investigation of 3.2-mm-diameter Orificed Hollow Cathodes," AIAA Paper 98-3798, July 1998.
[6] Siegfried, D. E., and Wilbur, P. J., "Studies on an Experimental Quartz Tube Hollow Cathode," AIAA Paper 79-2056, Oct. 1979.
[7] Salhi, A., "Theoretical and Experimental Studies of Orificed, Hollow Cathode Operation," Ph.D. Dissertation, The Ohio State Univ., 1993.
[8] Capacci, M., Minucci, M., and Severi, A., "Simple Numerical Model Describing Discharge Parameters in Orificed Hollow Cathode Devices," AIAA Paper 97-2791, July 1997.
[9] Van Noord, J. L., "Thermal Modeling of an Ion Thruster," Ph.D. Dissertation, Univ. of Michigan, 1999.
[10] Mikellides, I. G., Katz, I., Goebel, D. M., and Polk, J. E., "Hollow Cathode Theory and Experiment 2: A Two-Dimensional Theoretical Model of the Emitter Region," *Journal of Applied Physics*, Vol. 98, No. 11, 2005, p. 113303.
[11] Mikellides, I. G., Katz, I., Goebel, D. M., and Polk, J. E., "Theoretical Modeling of a Hollow Cathode Plasma for the Assessment of Insert and Keeper Lifetimes," AIAA Paper 05-4234, July 2005.
[12] Dushman, S., "Electron Emission from Metals as a Function of Temperature," *Physical Review*, Vol. 21, No. 6, 1923, pp. 623–636.
[13] Malik, A. K., Montarde, P., and Haines, M. G., "Spectroscopic Measurements of Xenon Plasma in a Hollow Cathode," *Journal of Physics D: Applied Physics*, Vol. 33, No. 16, 2000, pp. 2037–2048.
[14] Cronin, J. L., "Modern Dispenser Cathodes," *Proceedings of the IEEE*, Vol. 128, No. 19, 1981, p. 19.
[15] Siegel, R., and Howell, J. R., "Thermal Radiation Heat Transfer 4th Edition," Taylor & Francis, New York, 2002, pp. 226–227.
[16] Jameson, K., and Goebel, D., *41st AIAA/ASME/SAE/ASEE Joint Propulsion Conference*, AIAA Paper 05-3667, 2005.
[17] Forsythe, W. E., and Worthing, A. G., "Properties of Tungsten and the Characteristics of Tungsten Lamps," *Astrophysical Journal*, Univ. of Chicago Press, Vol. 61, 1924, pp. 146–185.
[18] Touloukian, Y. S., and DeWitt, D. P., *Thermophysical Properties of Matter*, Vol. 7, Plenum, New York, 1970.
[19] Polk, J. E., Marrese, C., Thornber, B., Dang, L., and Johnson, L., "Temperature Distributions in Hollow Cathode Emitters," AIAA Paper 04-4116, July 2004.
[20] Polk, J. E., Grubisic, A., Taheri, N., Goebel, D., Downey, R., and Hornbeck, S., "Emitter Temperature Distributions in the NSTAR Discharge Hollow Cathode," AIAA Paper 05-4398, July 2005.
[21] Polk, J. E., Anderson, J. R., Brophy, J. R., Rawlin, V. K., Patterson, M. J., Sovey, J., and Hamley, J., "Overview of the Results From an 8200 Hour Wear Test of the NSTAR Ion Thruster," AIAA Paper 99-2446, June 1999.

A. Gallimore
*Associate Editor*